Comparison of the luminescence properties of the x-ray storage phosphors $BaCl_2:Ce^{3+}$ and $BaBr_2:Ce^{3+}$

2005 J. Phys.: Condens. Matter 17 8069

(http://iopscience.iop.org/0953-8984/17/50/024)

INSTITUTE OF PHYSICS PUBLISHING JOURNAL OF PHYSICS: CONDENSED MATTER

J. Phys.: Condens. Matter **17** (2005) 8069–8078 doi:10.1088/0953-8984/17/50/024

Comparison of the luminescence properties of the x-ray storage phosphors $BaCl_2:Ce^{3+}$ and $BaBr_2:Ce^{3+}$

J Selling[1], G Corradi[1,2], M Secu[1,3] and S Schweizer[1,4]

[1] Department of Physics, University of Paderborn, Warburger Str. 100, D-33098 Paderborn, Germany
[2] Research Institute for Solid State Physics and Optics, Hungarian Academy of Sciences, Budapest, H-1525, Hungary
[3] National Institute of Materials Physics, Bucharest-Magurele, Romania

E-mail: schweizer@physik.upb.de

Received 29 July 2005, in final form 3 August 2005
Published 2 December 2005
Online at stacks.iop.org/JPhysCM/17/8069

Abstract

The single-crystalline x-ray storage phosphor $BaCl_2:Ce^{3+}$ has been investigated by photo- and x-ray luminescence, and also by observing the afterglow and the photostimulated luminescence (PSL). A single active Ce^{3+} site has been observed with a characteristic emission doublet at 349 and 373 nm at room temperature. The PSL stimulation spectrum shows a clear resemblance to F-type absorption spectra in undoped $BaCl_2$, indicating that the PSL-active electron centres are F-type centres. The results are compared with previous photoluminescence, PSL and new x-ray luminescence data on $BaBr_2:Ce^{3+}$. The integral PSL efficiency in the chloride is found to be somewhat smaller than in the bromide, which is still large enough for storage phosphor applications, while the efficiency in the bromide may be even larger or comparable to that of the commercial x-ray storage phosphor $BaFBr:Eu^{2+}$.

1. Introduction

Common x-ray films are increasingly being replaced by x-ray storage phosphor image plates. Theses plates store an x-ray latent image in the form of locally trapped electron–hole pairs. The stored information can be read out by photostimulated luminescence (PSL): upon excitation of the electron centres in their characteristic absorption bands in the visible spectral range, their electrons recombine with neighbouring hole centres resulting in a luminescence of a nearby doped activator which is usually a rare-earth activated ion (for a recent review, see [1]).

A disadvantage of the commercial x-ray storage phosphor $BaFBr:Eu^{2+}$ is its inferior spatial resolution in comparison to common x-ray films. Due to reduced light scattering, rare-earth activated and Br or Cl codoped fluorozirconate (ZBLAN) glass ceramics have a better spatial

[4] Author to whom any correspondence should be addressed.

resolution [2, 3]. These materials contain PSL-active BaX_2 (X = Cl, Br) nanocrystallites. These crystallites are formed in the glass ceramics upon appropriate annealing [4–8].

The investigation of the bulk BaX_2:Eu [9] and $BaBr_2$:Ce [10] phases yielded detailed information on efficient PSL processes not only active in these crystals but determining the PSL behaviour of the respective glassy systems as well. In this paper the studies are extended to Ce-doped $BaCl_2$ and the results are compared to those obtained for Ce-doped $BaBr_2$. Both crystals have isomorphous stable orthorhombic phases at room temperature (RT) [11].

2. Experiment

2.1. Sample preparation

Single crystals of orthorhombic $BaCl_2$ were grown in the Paderborn crystal growth laboratory using the Bridgman method with a quartz glass ampoule, $SiCl_4$ atmosphere and $BaCl_2$ powder to which 1000 molar ppm of $CeCl_3$ was added. The usual technique was modified using careful annealing and slow cooling through the cubic–orthorhombic phase transformation near 920 °C [11]. Prior to crystal growth the $BaCl_2$ powder was dried in vacuum with subsequent melting in $SiCl_4$ atmosphere to reduce oxygen contamination. X-ray diffraction measurements of the samples have shown the presence of the orthorhombic phase of $BaCl_2$ with no trace of the cubic or other phases detectable. Corresponding methods for the preparation of $BaBr_2$ single crystals have been described in a previous paper [10].

2.2. Experimental setup

The PL and PSL spectra were recorded with a single-beam spectrometer containing two 0.25 m double monochromators (Spex), one for excitation and another for emission. The samples were excited either with a halogen lamp for the visible spectral range or a xenon lamp for the ultraviolet range. The emission and excitation spectra were detected using a photomultiplier and single photon counting. The spectra were not corrected for spectral sensitivity of the experimental setup. The emission sensitivity is mainly due to the sensitivity of the photomultiplier and is relatively flat in the spectral range from around 390 up to 850 nm. Even in the region of decreasing sensitivity below 390 nm estimates show that the absolute emission peak positions given are reliable within a few nanometres, depending on the linewidth. Similar estimates, based on the spectral properties of the lamps and the spectral response of the monochromator, are valid for the excitation peaks and the components of the stimulation spectra. These small corrections would not qualitatively change any of the statements. For low-temperature measurements a continuous flow helium cryostat was used. For x-ray luminescence (XL) and prior to PSL measurements the samples were irradiated at RT or 20 K using a tungsten anode at 50 kV and 30 mA. The afterglow spectra were measured within 15 min after switching off the x-ray source. The PSL efficiency measurements were carried out using a 1 mW HeNe laser (632.8 nm) for stimulation and a photomultiplier with a 2 mm BG 3 band pass filter for integral detection in the 250–500 nm region.

3. Experimental results

3.1. Photoluminescence

Photoluminescence measurements performed at 20 K in $BaCl_2$:Ce^{3+} show a resolved luminescence doublet at 350 and 378 nm (figure 1, lower part, dashed curve; see also table 1).

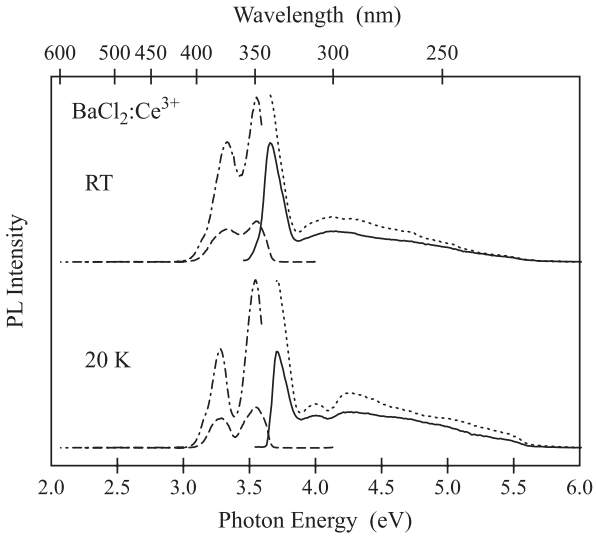

Figure 1. PL and PL excitation spectra of $BaCl_2:Ce^{3+}$. RT spectra (upper part): the PL was excited at 300 nm (dashed) and 339 nm (dash–dotted); the PL excitation was detected at 350 nm (dotted) and 373 nm (solid). 20 K spectra (lower part): the PL was excited at 290 nm (dashed) and 333 nm (dash–dotted); the PL excitation was detected at 349 nm (dotted) and 377 nm (solid).

Table 1. Wavelengths (nm) of the observed bands of the luminescent Ce^{3+} centre in orthorhombic $BaCl_2:Ce^{3+}$ (bold numbers indicate the most intense line(s) of the respective group).

Temp.	PL excitation	PL and XL emission	PSL emission	PSL stimulation	Reference
RT	234, **244**, 260, **274**, **316**, 325	337, 363			[13]
RT	220–320, **339**	**349**, 373	∼349, ∼373	516, ∼662	This work
20 K	220–290, 310, **334**	**350**, 378	349, 376	414–476–550, **660**	This work

The doublet shape is characteristic for the $5d^1 \rightarrow 4f^1$ emission of Ce^{3+}. The ∼2000 cm^{-1} splitting of this doublet is due to the spin–orbit splitting of the well-shielded ground state [12].

The excitation spectrum corresponding to the 378 nm peak, consisting of a more intense component at 334 nm, weaker ones at 310 nm and near 290 nm and several other, poorly resolved components extending to 220 nm, is also shown (figure 1, lower part, solid line). The excitation spectrum for the emission at 350 nm is essentially identical apart from somewhat changed intensity proportions of the components (dotted curve). Peaks in similar excitation spectra may result from the splitting of the fivefold degenerate $5d^1$ excited state of Ce^{3+} due to the crystal field and the spin–orbit interaction [12–14].

At RT all bands are slightly broadened, without essential changes. The luminescence doublet appears at 349 and 373 nm, (figure 1, upper part, dashed and dash–dotted curves); the excitation spectra corresponding to these peaks (dotted and solid lines in the upper part of figure 1, respectively) are slightly red-shifted, now consisting of a dominant peak at 339 nm and several weak, poorly resolved components between 220 and 320 nm.

Absorption in undoped $BaCl_2$ starts only above 7.5 eV, as was shown earlier in single-crystal films [15]. Therefore, host excitation for our PL experiments can be excluded. A much weaker photoluminescence in undoped $BaCl_2$ occurs only in the 400–500 nm region and will be described in a forthcoming paper [16].

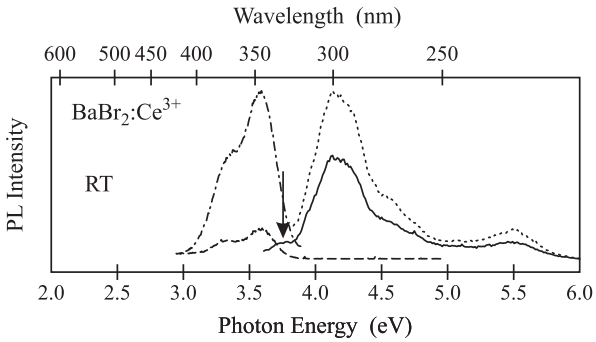

Figure 2. PL and PL excitation spectra of $BaBr_2$:Ce^{3+}. RT spectra: the PL was excited at 226 nm (dashed) and 300 nm (dashed–dotted); the PL excitation was detected at 345 nm (dotted) and 370 nm (solid).

For comparison with $BaBr_2$:Ce^{3+} the results of a similar measurement at RT for the A site are shown in figure 2. The only essential difference compared to previously published spectra [10] is the first small excitation peak at ∼327 nm, indicated with an arrow in figure 2 (solid curve, now detected at 370 nm). This peak is better resolved in the present experiment than in [10], where it was assumed to be near 308–310 nm.

3.2. X-ray luminescence and afterglow

The x-ray luminescence spectra in $BaCl_2$:Ce^{3+} are presented as solid lines in figure 3 for RT and 20 K. They contain the same Ce^{3+} emission doublet as seen in PL, only less resolved, especially at RT. In addition, there is also a smaller band near 300 nm attributed to the radiative decay of self-trapped excitons (STEs) in analogy to undoped $BaBr_2$ [17], and additional small bands in the 400–500 nm region are also present. These bands can also be observed in undoped $BaCl_2$ and will be described separately [16]. While at RT the dominance of the Ce^{3+} luminescence is overwhelming, at low temperatures the intrinsic luminescence, especially that of STEs, is appreciable. The afterglow (see dashed lines in figure 3) is dominated by the decay of the Ce^{3+} doublet, with the other bands again slightly enhanced at low temperature.

For comparison XL in $BaBr_2$:Ce^{3+} has also been investigated (see figure 4). Apart from minor shifts, the positions of the XL and afterglow bands are very similar to the case of $BaCl_2$:Ce^{3+}; however, there are changes of relative intensity, indicating changed efficiencies of various radiative decay channels. In addition to bands seen earlier in the XL of undoped $BaBr_2$ [17], Ce^{3+} bands at 350 and 370 nm at RT and 350 and 375 nm at 20 K also appear. Compared to intrinsic bands in the 400–500 nm region, the Ce^{3+} bands are again larger (but no more dominant) for both temperatures, while the STE band in the bromide seen at 20 K near 280 nm [17] dwarfs all other XL bands. The Ce^{3+} XL bands in question just correspond to the A-type PL (see figure 1 in [10]); the peak at 425 nm does not seem to belong to Ce but rather to some other defect, together with the 485 nm peak. In fact, the latter two emissions are seen in the PL and XL of undoped $BaBr_2$ as well (see dotted line in figure 4 and references [16, 17] for more detail). This means that the B-type luminescence may be small or absent in XL with the C-type emission also missing. The afterglow at RT in $BaBr_2$:Ce^{3+} is similar to the chloride case and comes from Ce^{3+}, but at 20 K the situation is completely reversed: because of the stronger decay of the Ce bands the other bands show a relative intensity larger by at least one order of magnitude (see the dashed curves in figure 4).

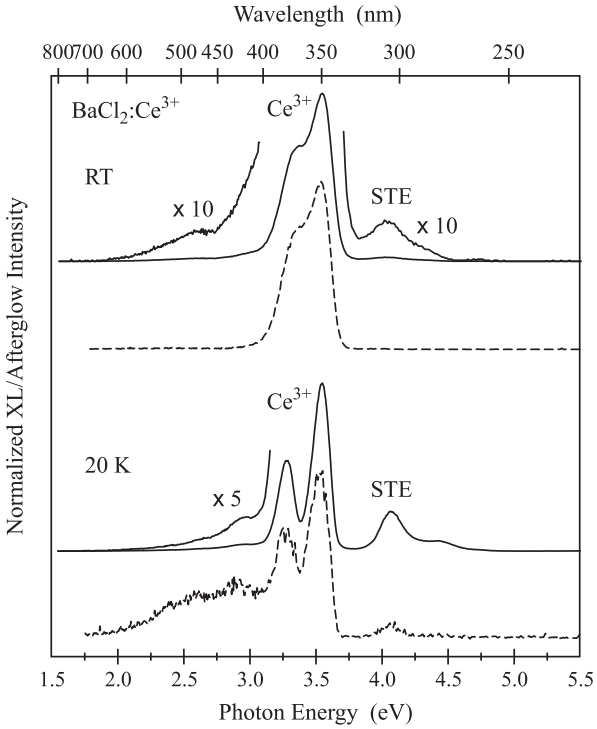

Figure 3. Normalized XL (solid curves) and afterglow spectra (dashed curves) of $BaCl_2:Ce^{3+}$, recorded at RT or 20 K (upper and lower parts, respectively). Parts of the XL spectra are also magnified 5 or 10 times as indicated. The spectra are vertically displaced for the sake of clarity.

3.3. Photostimulated luminescence

The PSL spectrum of $BaCl_2:Ce^{3+}$ measured following x-irradiation at RT again shows a doublet at 349 and 376 nm (figure 5, solid curves), which is similar to the doublet seen in PL and XL. At RT there is very small further broadening of the lines compared to XL. Observing the PSL at 20 K only slightly improves spectral resolution, in contrast to XL and PL where the doublet is much better resolved at low temperature (compare the Ce^{3+} doublets in figures 1, 3 and 5).

The PSL stimulation spectra detected at 350 nm (dashed curves in figure 5) show clear resemblance to the F-centre absorption spectrum in undoped $BaCl_2$ [18] and our absorption spectra taken in $BaCl_2:Eu^{2+}$ [9]. The stimulation maxima appear at ∼645, ∼575, ∼510, and ∼470 nm (20 K), while the F-centre absorption has only three maxima at 645, ∼555 and 500 nm, corresponding to the A, B, C, and D transitions where B and C are weakly resolved. However, in $BaBr_2:Ce^{3+}$ the F-type broad stimulation spectrum of the A-type PSL had a blueshift of ∼70 nm compared to the similarly shaped and unshifted B-type PSL [10]. Therefore we assume, that in the chloride we see a mixed spectrum due to several differently perturbed F-type centres. Compared to the F-centre absorption maxima the components of the PSL stimulation spectrum are broadened and poorly resolved, especially at RT, with minor variations of relative intensity and position depending on sample orientation and position.

The decay properties and especially the integral efficiency of the PSL at RT are crucial for storage phosphor applications [1]. We carried out preliminary read-out experiments for $BaBr_2:Ce^{3+}$, $BaCl_2:Ce^{3+}$, and $BaFBr:Eu^{2+}$ single crystals by measuring the PSL intensity over practically the full decay (in our case up to 3 h bleaching time), using in each case the same

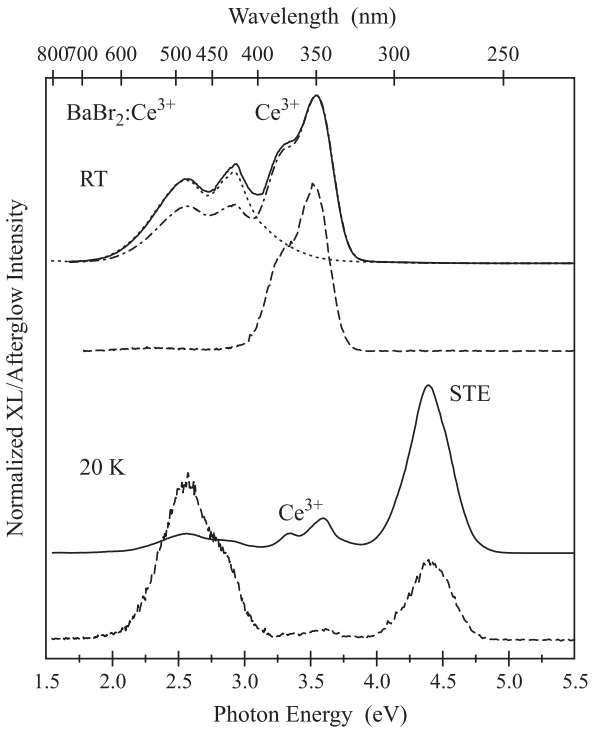

Figure 4. Normalized XL (solid curves) and afterglow (dashed curves) spectra of $BaBr_2:Ce^{3+}$, recorded at RT or 20 K (upper and lower parts, respectively). The XL at RT is also shown for another $BaBr_2:Ce^{3+}$ sample (dash–dotted) and for undoped $BaBr_2$ (dotted). The spectra are vertically displaced for the sake of clarity.

1 mW HeNe laser (632.8 nm) for stimulation and the same band pass filter (BG 3) for detection. All samples were x-irradiated and read out under the same conditions for the same time. As shown in figure 6, at RT the decay of the PSL is multi-exponential, and can be characterized by a continuous distribution of time constants. The starting slope for $BaCl_2:Ce^{3+}$ is comparable to that of $BaFBr:Eu^{2+}$ and corresponds to a time constant of a few minutes in our case, while for $BaBr_2:Ce^{3+}$ the initial time constant is roughly three times longer. It should be noted that in the case of the Eu activator the bromide also showed slower bleaching than the chloride [9], despite the larger absorption constant in the bromide sample at the stimulation wavelength 570 nm used in that work.

The overall efficiency of the PSL was estimated by integrating the curves in figure 6 over the full decay measured. In $BaCl_2:Ce^{3+}$, the integrated intensity found is about 30% of that measured for the $BaFBr:Eu^{2+}$ emission. The PSL efficiency of $BaBr_2:Ce^{3+}$ is found to be about 55% of that of $BaFBr:Eu^{2+}$. The precision of these ratios is limited by the hygroscopic character of the samples, especially in the case of $BaBr_2$. It should be noted that laser light with a wavelength of 632.8 nm is not the best read-out wavelength for $BaCl_2:Ce^{3+}$ (see figure 5) and $BaBr_2:Ce^{3+}$ [10], while for $BaFBr:Eu^{2+}$ it is nearly optimal. Compared to green laser stimulation (which would reverse the situation) the mismatch cuts out the major part of the more important A-type luminescence in the bromide (at RT), and also appreciably reduces the B-type emission in the bromide and the single type in the chloride. Taking into account all circumstances, our estimates indicate that for $BaBr_2:Ce^{3+}$ a PSL efficiency exceeding or

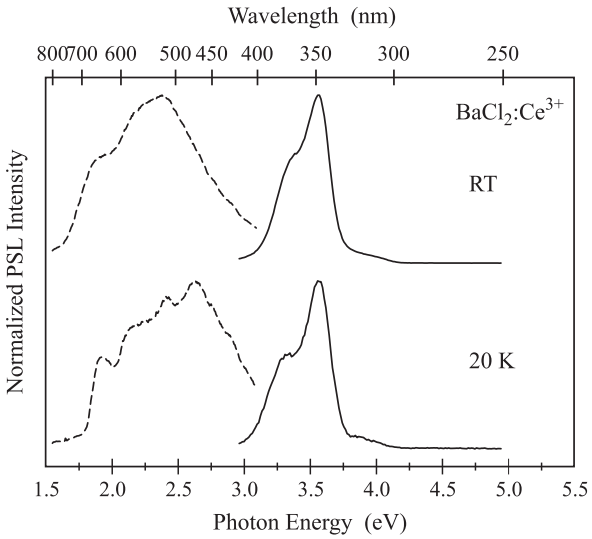

Figure 5. PSL and PSL stimulation spectra of $BaCl_2:Ce^{3+}$: (a) after x-irradiation at RT, recorded at RT, and (b) after x-irradiation at RT, recorded at 20 K. The PSL (solid curves) was stimulated at 550 nm, the PSL stimulation (dashed curves) was detected at 350 nm. The spectra are vertically displaced for the sake of clarity.

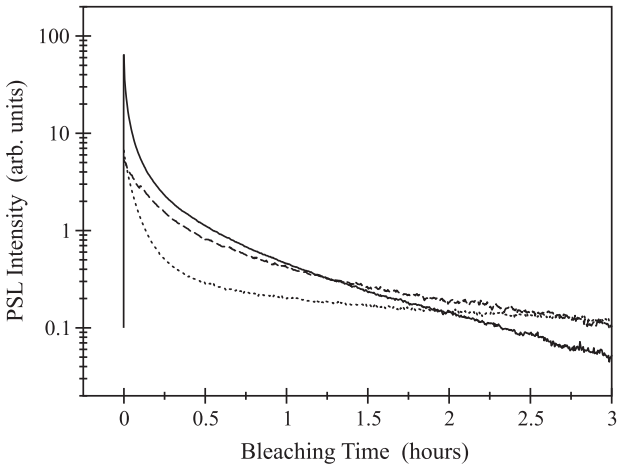

Figure 6. PSL decay curves of $BaBr_2:Ce^{3+}$ (dashed curve), $BaCl_2:Ce^{3+}$ (dotted curve), and $BaFBr:Eu^{2+}$ (solid curve) under continuous stimulation with 632.8 nm light of a HeNe laser, recorded at RT. The PSL intensity was detected integrally using a 2 mm BG 3 band pass filter after x-irradiation at RT.

comparable to that of $BaFBr:Eu^{2+}$ can be achieved, while for $BaCl_2:Ce^{3+}$ the efficiency is still large enough for storage phosphor applications.

4. Discussion

The band positions characterizing the active Ce^{3+} site in $BaCl_2$ single crystals are compiled in table 1 together with earlier RT data of Li and Leskelä [13] obtained for $BaCl_2$ powder doped

Table 2. Parameter values for Ce^{3+} luminescence in various matrices: number (N) and average unrelaxed distance (R_{av}) of ligands [11], wavelength of the first f–d transition in PL excitation or absorption ($\lambda_{exc/abs}$), the same in emission (λ_{em}), total apparent d–d splitting (ε_{cfs}), redshift (D) of the first absorption transition with respect to the emission at 202.67 nm of the free Ce^{3+} ion, and the Stokes shift (ΔS). The spectroscopic data refer to 20 K unless indicated by the index RT.

Comp./Site	N	R_{av} (pm)	$\lambda_{exc/abs}$ (nm)	λ_{em} (nm)	ε_{cfs} (cm^{-1})	D (cm^{-1})	ΔS (cm^{-1})	Reference
$BaCl_2$ (cubic)	8	329	334^{RT}	352^{RT}	$\sim 12\,610^{RT}$	$19\,400^{RT}$	1531^{RT}	[13]
$BaCl_2$ (ortho.)	9	324	325^{RT}	337^{RT}	$\sim 12\,000^{RT}$	$18\,571^{RT}$	1095^{RT}	[13]
$BaCl_2$ (ortho.)								This work
	9	324	339^{RT}	349^{RT}	$\sim 14\,000^{RT}$	$19\,840^{RT}$	850^{RT}	
	9	324	334	350	$\sim 14\,500$	19 390	1370	
$BaBr_2$ (ortho.)								
A	9	341	327^{RT}	345^{RT}	$12\,897^{RT}$	$18\,760^{RT}$	1596^{RT}	This work
B[a]	9	341	305(?)	382	$>10\,000$	16 553(?)	6610(?)	[10]
C	9	341	302	330	7851	16 228	2810	[10]

[a] Overlap with bands not related to Ce making some assignations insecure.

with 0.05–0.5% Ce. The main parameters are summarized in table 2. Our single-crystal RT data are only roughly comparable to those of Li and Leskelä; the difference may be attributed to the fact that we have single crystals. At 20 K we have much better resolution for the emission, which is now clearly seen to be a simple doublet essentially corresponding to a single Ce^{3+} site. There is a most prominent lowest energy PL excitation peak at 334 nm (339 nm at RT), compared to a weaker maximum at 316 nm with a shoulder near 325 nm presented in [13]. The rest of the excitation spectrum, however, remains rather unresolved even at 20 K, in contrast to our low-temperature results in $BaBr_2$ [10].

For the less hygroscopic $BaCl_2$:Ce^{3+} a clearly larger part of the luminescence comes from Ce compared to $BaBr_2$:Ce^{3+}, where luminescence related to oxygen centres is also important [10]. For $BaCl_2$ the Stokes shift ΔS has a moderate value of $\sim 1370\ cm^{-1}$ at 20 K which is much smaller than possible values expected for the presumably oxygen compensated B-site in $BaBr_2$. Apart from worse resolution, the new data are much closer to those obtained for the Ce^{3+} A-site in $BaBr_2$ (see table 2). The repeated PL measurements for $BaBr_2$:Ce^{3+} lead to a minor correction of the first A-type excitation peak, stressing the similarity between the bromide A-site and the site in the chloride.

Compared to Li and Leskelä [13], our measurements give slightly increased values for the redshift D in orthorhombic $BaCl_2$:Ce^{3+} (see table 2). So the D value for the chloride remains larger than that found for the bromide, in contrast to lanthanum and lutetium salts; however, these comparisons may also be affected by the fact that La salts have smaller and the Lu ones clearly larger apparent d–d splittings than the Ba salts (see [10] and [14]).

The differences in the PL excitation spectra of the chloride and bromide, and in particular the lack of resolution in $BaCl_2$:Ce^{3+} indicate that the picture of a single active Ce site in the chloride still may hide various more or less different Ce sites. Part of these sites may even be inactive in emission due to energy transfer to the active ones. So the simpler PL emission properties in the chloride do not obviously indicate a simple defect structure. Note that the lattice constants of the chloride and bromide differ by only 5% [11].

In K- or Na-codoped $BaCl_2$:Ce^{3+}, Li and Leskelä observed more intense luminescence than without these codopants, without any appreciable shift of the bands [13]. This supports the assumed assignation to emitting Ce^{3+} sites charge-compensated by monovalent cations.

The XL measurements have shown how efficient the Ce^{3+} activator is in collecting the radiation energy at RT, though other channels are also available [16]. At 20 K the energy transfer to Ce^{3+} is weaker; while this is a small change in $BaCl_2$, in $BaBr_2$ the transfer to Ce^{3+} is nearly quenched at low temperature. One cause for energy transfer is partial reabsorption of the STE emission overlapping with the Ce^{3+} excitation bands. At RT the overlap is enhanced due to the observed temperature broadening of both overlapping partners. Other mechanisms related for example to the temperature-dependent mobility of the STEs and charge carriers may also contribute to the energy transfer. According to our experiments all transfer mechanisms are rather inefficient in the bromide at low temperature. The presence of radiation defects also contributes to the line broadening of the XL and afterglow, explaining their broadening compared to PL as observed especially at RT. More information on transfer efficiencies, interactions and trapping processes may be expected from time-resolved luminescence measurements.

The stable PSL-active electron trap centres have been found, similarly to all activated barium halide systems investigated to date ($BaFBr:Eu^{2+}$ [19, 20], $BaFCl:Eu^{2+}$ [19], $BaBr_2:Eu^{2+}$ [9], $BaCl_2:Eu^{2+}$ [9] and $BaBr_2:Ce^{3+}$ [10]), to be F-centres. In $BaCl_2:Ce^{3+}$ as well they seem to be of various kinds.

The fact that they belong to the same Ce^{3+} doublet may be described in a number of somewhat different PSL scenarios involving one or more types of nearby hole centres where recombination and STE formation takes place [17] and one or more types of nearby Ce^{3+} site where the energy is transferred to. If more than one type of Ce^{3+} site is assumed, an energy transfer from one type to the other or coinciding emission bands also have to be postulated, since only one emission doublet is observed. An indication for the participation of mute Ce^{3+} sites in the energy transfer was given by the unresolved PL excitation spectrum discussed above.

The broadening of stimulation sub-bands and of the PSL doublet (with respect to absorption and XL, respectively), observed even at 20 K, indicate that most partners involved in the PSL process are perturbed, similarly to the case of the other barium halide systems [9, 10, 20]. As concluded in these works, most PSL-active radiation defects are stabilized near rare-earth sites (the expected separations being of the order of a few lattice constants [20]) which means sources of perturbation for all involved partners: in particular for the active rare-earth sites yielding the PSL and the electrons trapped as perturbed F-centres and showing up in PSL stimulation. Similar perturbations are expected for the hole centres [1, 10, 17] which, however, could not be observed in the present experiments. The main difference between the Eu^{2+} and Ce^{3+} activated systems is that Ce^{3+} usually also requires charge compensation which means further perturbation and line broadening. This also explains the more complex structure of the PSL stimulation spectra observed both for $BaCl_2:Ce^{3+}$ and $BaBr_2:Ce^{3+}$ [10], compared to the Eu^{2+}-doped cases [9] where they are nearly identical with the (essentially activator independent) absorption spectrum. The different variants of charge-compensation geometry may also contribute to the multi-exponential character of the PSL decay curve observed for both the chloride and bromide (figure 6). However, even in the absence of charge compensation several components in the PSL decay curves may occur: different time constants may be due to F-centres located at different distances from the rare-earth hole pairs as suggested previously for $BaFBr:Eu^{2+}$, $BaBr_2:Eu^{2+}$ and $BaCl_2:Eu^{2+}$ [9, 21]. The slower bleaching process in $BaBr_2$ compared to $BaCl_2$ observed for both activators may be attributed to the larger stability of the F-centres in the bromide against the stimulations used, the process depending on a number of factors, including centre distributions. Independent of these minor differences, the observed integral PSL efficiency for both $BaCl_2:Ce^{3+}$ and $BaBr_2:Ce^{3+}$ is large enough for storage phosphor applications.

5. Conclusion

We have shown that in orthorhombic $BaCl_2$:Ce^{3+}, in contrast to orthorhombic $BaBr_2$:Ce^{3+}, there is only a single type of light-emitting Ce site. The properties of this site come rather close to those of the A-site in the bromide, which could be attributed to Ce^{3+} on a Ba^{2+} site charge-compensated by a monovalent impurity cation. The PSL-active electron traps are again variously perturbed F-centres. As a consequence of non-uniform inter-defect distances and various charge-compensation configurations the PSL has a bleaching behaviour characterized by multi-exponential decay on the minute scale both for the chloride and the bromide. The integral efficiency of the PSL of both Ce salts is large enough for applications; in fact, for the bromide it is at least comparable to that of the well-known phosphor BaFBr:Eu^{2+}, making them prospective x-ray storage materials if properly encapsulated, for example in a glass matrix.

Acknowledgments

The authors are indebted to the Deutsche Forschungsgemeinschaft and also to the Hungarian Scientific Research Fund (OTKA T 034262 and 60086) for financial support.

References

[1] Schweizer S 2001 *Phys. Status Solidi* a **187** 335
[2] Edgar A, Williams G V M, Schweizer S and Spaeth J-M 2005 *Curr. Appl. Phys.* at press
[3] Chen G, Johnson J A, Weber R, Schweizer S, MacFarlane D, Woodford J and De Carlo F 2005 *Proc. SPIE* **5745** 1351
[4] Edgar A, Spaeth J-M, Schweizer S, Assmann S, Newman P J and MacFarlane D R 1999 *Appl. Phys. Lett.* **75** 2386
[5] Edgar A, Secu M, Williams G V M, Schweizer S and Spaeth J-M 2001 *J. Phys.: Condens. Matter* **13** 6259
[6] Secu M, Schweizer S, Spaeth J-M, Edgar A, Williams G V M and Rieser U 2003 *J. Phys.: Condens. Matter* **15** 1097
[7] Schweizer S, Hobbs L W, Secu M, Spaeth J-M, Edgar A and Williams G V M 2003 *Appl. Phys. Lett.* **83** 449
[8] Schweizer S, Hobbs L W, Secu M, Spaeth J-M, Edgar A, Williams G V M and Hamlin J 2005 *J. Appl. Phys.* **97** 083522
[9] Secu M, Kalchgruber R, Schweizer S, Spaeth J-M and Edgar A 2002 *Radiat. Eff. Defects Solids* **157** 957
[10] Corradi G, Secu M, Schweizer S and Spaeth J-M 2004 *J. Phys.: Condens. Matter* **16** 1489
[11] Brackett E B, Brackett T E and Sass R L 1963 *J. Phys. Chem.* **67** 2132
[12] Blasse G and Grabmaier B C 1994 *Luminescent Materials* (Berlin: Springer)
[13] Li W-M and Leskelä M 1996 *Mater. Lett.* **28** 491
[14] Dorenbos P 2001 *Phys. Rev.* B **64** 125117
[15] Nicklaus E 1979 *Phys. Status Solidi* a **53** 217
[16] Selling J, Corradi G, Secu M and Schweizer S 2006 *J. Phys.: Condens. Matter* in preparation
[17] Secu M, Schweizer S, Rogulis U and Spaeth J-M 2003 *J. Phys.: Condens. Matter* **15** 2061
[18] Houlier B 1977 *J. Phys. C: Solid State Phys.* **10** 1419
[19] Takahashi K, Miyahara J and Shibahara Y 1985 *J. Electrochem. Soc.* **132** 1492
[20] Koschnick F K, Spaeth J-M and Eachus R S 1992 *J. Phys.: Condens. Matter* **4** 8919
[21] Hangleiter T, Koschnick F K, Spaeth J-M, Nuttall R H D and Eachus R S 1990 *J. Phys.: Condens. Matter* **2** 6837